Journal of Molecular Structure 998 (2011) 20–29

Contents lists available at ScienceDirect

Journal of Molecular Structure

journal homepage: www.elsevier.com/locate/molstruc

Synthesis, characterization, molecular modeling and antibacterial activity of $N^{1'}$, $N^{2'}$-bis[1-(pyridin-2-yl)ethylidene]oxalohydrazide and its metal complexes

O.A. El-Gammal, R.M. El-Shazly, F.E. El-Morsy, A.A. El-Asmy *

Department of Chemistry, Faculty of Science, Mansoura University, Mansoura, Egypt

ARTICLE INFO

Article history:
Received 26 February 2011
Received in revised form 28 April 2011
Accepted 28 April 2011
Available online 5 May 2011

Keywords:
Hydrazide
Spectra
Molecular modeling
Antimicrobial activity

ABSTRACT

New complexes of $N^{1'}$,$N^{2'}$-bis[1-(pyridin-2-yl)ethylidene]oxalohydrazide (H_2L) with Cr^{3+}, Mn^{2+}, Fe^{3+}, Co^{2+}, Ni^{2+}, Cu^{2+}, Cd^{2+}, VO^{2+} and Ag^{+} have been prepared and characterized. The ligand has 10–12 buffering range and pK's of 4.62, 7.78 and 9.45. The IR spectra showed the neutral, (mono- or dibasic) bidentate, tridentate or tetradentate of H_2L. The molar conductance values, in DMSO, are in the range of nonelectrolytes. An octahedral geometry is proposed for the Cr^{3+}, Mn^{2+}, Fe^{3+}, Ni^{2+}; VO^{2+} complexes and square–planar for the Co^{2+} and Cu^{2+} complexes. The ESR spectra support the mononuclear species for $[VO(H_2L)SO_4\_(H_2O)_2]\cdot H_2O$ and $[Cu(H_2L)(OAc)_2]\cdot H_2O$. The molecular parameters have been calculated to confirm the geometry of the ligand and its complexes. The ligand and some complexes were screened against *Bacillus thuringiensis* (Bt) as Gram positive and *Pseudomonas aeuroginosa* (Pa) as Gram negative bacteria using the inhibitory zone diameter. The data showed no effect for the complexes on Pa bacteria growth except $[Ag(H_2L)(NO_3)]H_2O$ which had a high activity. Cu^{2+}, VO^{2+} and Ag^{+} complexes exhibit activity against BT; Cu^{2+}complex is the highest one.

1. Introduction

Hydrazide derivatives constitute very important class of NO donors due to their capability and structural flexibility which provide rigidity to the skeletal framework of the prepared multinuclear complexes. Systematic investigation of the transition metal complexes of these compounds revealed interesting electrical, magnetic properties and pharmacological activities [1,2]. The hydrazone complexes exhibit some intriguing structural features owing to the potency of the ligand to act in a planar pentadentate fashion [3–6] along with the tridentate character [6,7–10]. Moreover, the ligands exhibit keto-enol tautomerism and can coordinate as neutral [5], monoanionic [11], dianionic [3,12,13] or tetraanionic [14] bearing unusual coordination numbers [3,15] in some mononuclear or binuclear species depending on the metal ion concentration, the medium pH and the nature of hydrazone.

Continuation to our previous work [16,17], the present work aims to prepare and characterize $N^{1'}$,$N^{2'}$-bis[1-(pyridin-2-yl)ethylidene]oxalohydrazide and its complexes. Thermal behavior of the isolated complexes was discussed. The pH and solvent effects on the ligand was studied. Finally, the antibacterial activity of the ligand and its complexes was tested.

2. Experimental

2.1. Materials

$VOSO_4\cdot H_2O$, $Cr_3(OAc)_7(OH)_2$, $MnCl_2\cdot 4H_2O$, $CoCl_2\cdot 6H_2O$, $Co(OAc)_2\cdot 4H_2O$, $NiCl_2\cdot 6H_2O$, $Ni(OAc)_2\cdot 4H_2O$, $CuCl_2\cdot 2H_2O$ $Cu(OAc)_2\cdot H_2O$ and $Cd(OAc)_2\cdot 2H_2O$ were Aldrich or Fluka products and used without further purification.

2.2. Synthesis of 2,2-$N^{1'}$,$N^{2'}$-bis(1-(pyridin-2-yl)ethylidene) oxalohydrazide (H_2L)

It was prepared by heating 1:2 M ratio of oxalohydrazide (1.18 g, 0.01 mol) and 2-acetylpyridine (2.24 ml, 0.02 mol) in 30 ml hot ethanol. The reaction mixture was boiled under reflux for 3 h, evaporated and after cooling, white crystals of H_2L (Structure 1) were formed. The precipitate was filtered off, recrystallized from ethanol and finally dried in a vacuum desiccator over anhydrous $CaCl_2$. The purity was checked by TLC. The melting point is 261 °C (yield is 78%).

2.3. Synthesis of the metal complexes

A hot ethanol or aqueous-ethanol solution of metal acetate [Co(II), Ni(II), Cd(II)] or $CrCl_3$, $MnCl_2$, $FeCl_3$, $AgNO_3$ (1.0 mmol) and $VOSO_4$ (2.0 mmol), was added to a hot ethanol of H_2L (0.324 g, 1.0 mmol). The resultant mixture was heated under reflux

---

* Corresponding author. Tel.: +020101645966.
E-mail address: aelasmy@yahoo.com (A.A. El-Asmy).

0022-2860/$ - see front matter © 2011 Elsevier B.V. All rights reserved.
doi:10.1016/j.molstruc.2011.04.043

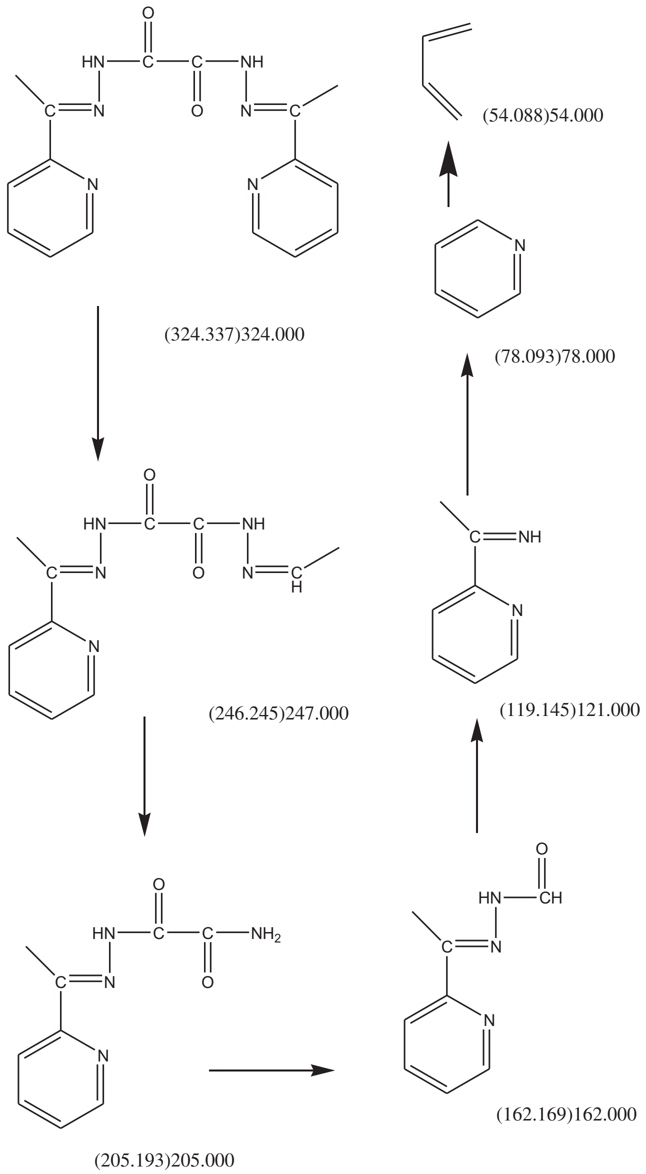

Scheme 1. Fragmentation pattern for H_2L.

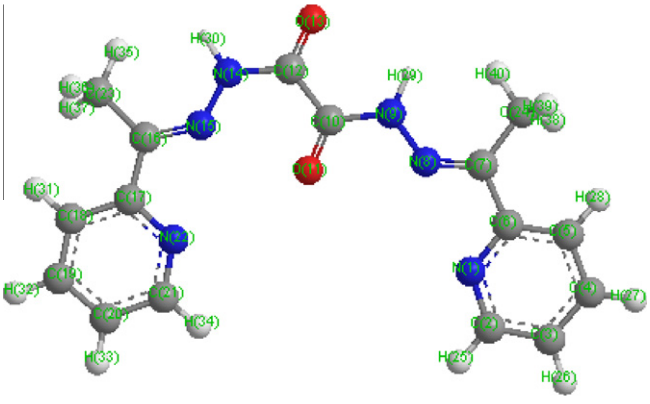

Structure 1. Molecular modeling of H_2L.

for 2–3 h. The formed precipitates were filtered off, washed with ethanol followed by diethyl ether and dried. The complexes, $[Cu(H_2L)(OAc)_2]\cdot H_2O$ and $[Cu_2(L)(OAc)_2(H_2O)_2]\cdot 3H_2O$ were isolated by mixing of $Cu(OAc)_2$ and ligand solutions in molar ratio 1:1 and 3:1 (M:L), respectively, with yield of 70–93%. The physical and analytical data of the isolated complexes are listed in Table 1. The complexes have high melting points (>300 °C), insoluble in common organic solvents and soluble in DMSO and DMF except for the Co(II) and Ni(II) complexes which are partially soluble. Molar conductance values indicate a non-electrolytic nature of the complexes [18]; the relative high value measured for $[Fe(H_2L)Cl_3]\cdot H_2O$ (46.36 L mol^{-1} cm^{-1}) may be due to solvolysis.

2.4. Analysis and Instrumentation

Elemental analyses (C, H, N) were performed with a Perkin–Elmer 2400 series II analyzer. Molar conductance values (10^{-3} mol L^{-1}) of the complexes, in DMSO, were measured using a Tacussel conductivity bridge model CD6NG. IR spectra (4000–400 cm^{-1}) were recorded on a Mattson 5000 FTIR spectrophotometer. Electronic spectra were recorded on a Unicam UV–Vis spectrophotometer UV_2. ^1H NMR measurements in d6-DMSO at room temperature were carried out on a Varian Gemini WM-200 MHz spectrometer at the Microanalytical Unit, Cairo University. The ESR spectra of Cu^{2+} and VO^{2+} complexes were recorded on a Bruker EMX spectrometer working in the X-band (9.78 GHz) with 100 kHz modulation frequency. The microwave power and modulation amplitudes were set at 1 mW and 4 Gauss, respectively. The low field signal was obtained after four scans with 10 folds increase in the receiver again. A powder spectrum was obtained in a 2 mm quartz capillary at room temperature. Magnetic susceptibilities were measured with a Sherwood scientific magnetic susceptibility balance at 298 K. Thermogravimetric measurements (TGA, DTA, 20–1000 °C) were recorded on a DTG-50 Shimadzu thermogravimetric analyzer at a heating rate of 10 °C/min and nitrogen flow rate of 20 ml/min.

2.5. Molecular modeling

An attempt to gain a better insight on the molecular structure of the ligand and its complexes, geometric optimization and conformational analysis has been performed by the use of MM+ force field as implemented in hyperchem 8.0 [20]. Semi empirical method PM3 is then used for optimizing the full geometry of the system using Polak–Ribiere (conjugate gradient) algorithm and Unrestricted Hartee–Fock (UHF) is employed keeping RMS gradient of 0.01 kcal/Å mol.

2.6. Antibacterial activity

The *in vitro* antibacterial activity of H_2L and its complexes was evaluated against *Bacillus thuringiensis* (*Bt*) as Gram positive bacterium and *Pseudomonas aeuroginosa* (*Pa*) as Gram negative bacterium using streptomycin as a control. The hole plate diffusion method [19] was adopted for the activity measurements. The bacterial strains were grown in nutrient agar slants. A suspension of the studied compounds (0.2 ml of each (10 μg/ml) was incubated at 36 °C for 36 h for the bacterial culture. After inoculation, the diameter (in mm) of the clear inhibition zone surrounding the sample is taken as a measure of the inhibition power against the particular organisms. The experiments were repeated three times and the values recorded are the mean average.

Table 1
Analytical and physical data of H_2L and its metal complexes.

Compound empirical formula	Yield (%)	Color	M.P. (°C)	% Found (Calcd.)				Λ° in DMSO
				C	H	M	Cl	
H_2L $C_{16}H_{16}N_6O_2$	93	White	261	59.88 (59.25)	5.36 (4.97)	–	–	–
$[Cu(H_2L)(OAc)_2]\cdot H_2O$ $CuC_{20}H_{24}N_6O_7$	80	Brownish green	>300	45.75 (45.84)	5.09 (5.00)	12.02 (12.12)	–	2..51
$[Cu_2(L)(OAc)_2(H_2O)_2]\cdot 3H_2O$ Cu_2 $C_{20}H_{30}N_6O_{11}$	70	Dark green	>300	36.50 (36.53)	5.04 (4.59)	19.39 (19.32)	–	–
$[Co_2L(OAc)_2(H_2O)_2]\cdot H_2O$ $Co_2C_{20}H_{26}N_6O_9$	81	Dark Brown	>300	39.59 (39.28)	4.54 (4.28)	18.80 (19.26)	–	–
$[Ni(HL)_2(H_2O)_2]\cdot H_2O$ $NiC_{32}H_{36}N_{12}O_7$	80	Reddish brown	>300	50.77 (50.61)	4.40 (4.77)	8.02 (7.73)	–	–
$[Fe(H_2L)Cl_3]\cdot H_2O$ $FeC_{16}H_{18}N_6O_3Cl_3$	88	Brown	Ch. 270	38.20 (38.08)	3.61 (3.59)	11.42 (11.06)	21.30 (21.07)	46.36
$[Cr(H_2L)Cl_3]\cdot 2H_2O$ $CrC_{16}H_{20}N_6O_4Cl_3$	86	Pale green	>300	37.47 (37.05)	4.00 (3.88)	10.00 (10.02)	20.14 (20.50)	16.03
$[Mn(H_2L)Cl_2(H_2O)]\cdot H_2O$ $MnC_{16}H_{22}N_6O_4Cl_2$	82	Orange	>300	39.77 (39.52)	4.47 (4.14)	11.60 (11.29)	15.00 (14.58)	35.64
$[VO(H_2L)SO_4(H_2O)]\cdot 2H_2O$ $VOC_{16}H_{22}N_6O_5SO_4$	85	Pale Green	>300	35.46 (35.49)	4.02 (4.09)	–	–	19.85
$[Cd(HL)(OAc)(EtOH)]EtOH$ $CdC_{22}H_{30}N_6O_6$	75	Yellow	>300	45.64 (45.02)	3.67 (5.15)	18.77 (19.15)	–	1.00
$[Ag(H_2L)NO_3]\cdot H_2O$ $AgC_{16}H_{18}N_7O_6$	78	Gray	265–270	37.40 (37.51)	4.70 (3.54)	21.27 (21.05)	–	27.32

3. Results and discussion

The data of elemental analysis together with some physical properties of the complexes are summarized in Table 1.

3.1. Molecular modeling

The molecular modeling of H_2L and its metal complexes drawn in structures (1–11) showed the following: (i) a large variation in the N_8—N_9 bond length on coordination *via* $N_{azomethine}$ and C—O; N_1—C_6 length becomes more shorter in $[Cu_2(L)(OAc)_{2-}(H_2O)_2]\cdot 3H_2O$ [21]. (ii) The C_{10}—O_{11} and C_{12}—O_{13} distances in all complexes become shorter except for $[Co_2L(OAc)_2]\cdot 3H_2O$ and $[Cu_2L(OAc)_2(H_2O)_2]\cdot 3H_2O$ in which the bond is enlongated referring to the formation of M—O [22]. (iii) The distance remains unaltered in $[Ag(H_2L)(NO_3)]\cdot H_2O$ and $[Cu(H_2L)(OAc)_2]\cdot H_2O$. (iv) The bond angles of hydrazone moiety are altered somewhat upon coordination. (v) The large change affects the N_8—N_9—C_{10}, N_9—C_{10}—O_{11} and O_{11}—C_{10}—C_{12} angles [21]. (vi) The N_8—N_9—C_{10} angle changes from 119.5° to (108.7–121.9°) in all complexes due to the formation of N_8—M—O_{11} ring [22]. (vii) The bond angles in $[Cr(H_2L)Cl_3]\cdot 2H_2O$, $[Mn(H_2L)(H_2O)Cl_2]\cdot H_2O$ and $[Fe(H_2L)(H_2O)Cl_3]\cdot H_2O$, $[Ni(HL)_{2-}(H_2O)_2]\cdot H_2O$ and $[VO(H_2L)(SO_4)(H_2O)]\cdot 2H_2O$ are quite near an octahedral geometry. (viii) The bond angles in $[Cu(H_2L)(OAc)_2]\cdot H_2O$ and $[Co_2L(OAc)_2]\cdot 3H_2O$ lie in the range reported for a square–planar geometry; the lower HOMO values showed that the molecules donating electron ability are weak. (ix) The high HOMO energy implies that the molecules are good electron donors; LUMO energy presents the ability of a molecule to receive electron [23]. (x) The bond angle within the hydrazone backbone did not change significantly but the angle around the metal undergoes appreciable variations upon changing the metal center [24].

3.2. IR and ^{1}H NMR spectra

The most important IR bands of H_2L (Structure 1) and its complexes are given in Table 2. The ligand has multi coordination sites which gave variable coordination modes. Its spectrum shows two bands at 1593 and 1575 cm^{-1} assignable to $\nu(C{=}N)_{azomethine}$ and $\nu(C{=}N)_{pyridine}$ [25] while the strong band at 1693 cm^{-1} is attributed to $\nu(C{=}O)$. The medium band at 3342 cm^{-1} is attributed to $\nu(NH)$ [21] while the band at 1060 cm^{-1} is due to $\nu(N{-}N)$ [26]. The absence of bands at 1800–1960 and 2300–2400 cm^{-1} proves no intramolecular hydrogen bonding (N—H···O) [27].

The ^{1}H NMR spectrum of H_2L, in d_6-DMSO solution (Fig. 1) suggests the existence of the ligand in the enol form as evidenced by the appearance of signals at $\delta = 15.8$, 11.8 and 11.6 ppm assignable to the protons of OH (due to the enolization of one carbonyl group) and NH. The signal attributed to the methyl protons (6H) is appeared at 2.32 ppm while those of pyridine rings (8H) are observed as multiple peaks at 7.34 [t, 2H (H—C5; H—C18)], 7.72 [d, 2H (H—C4; H—C19)], 7.77 [d, 2H (H—C3; H—C20)] and 8.52 ppm [d, 2H (H—C6; H—C17)] [28]; the numbering of the atoms in the ligand is shown as follows:

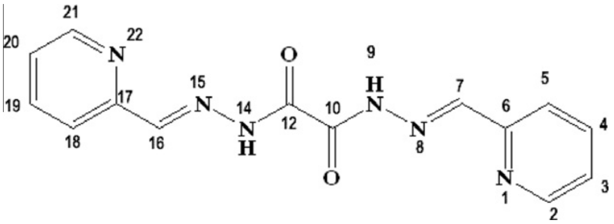

H_2L behaves in $[Ag(H_2L)(NO_3)]\cdot H_2O$ (Structure 2) as a neutral monodentate coordinating *via* $C{=}N_{azoethine}$ as indicated by the shift of its band to higher wavenumber [24–26]. The spectrum shows two bands at 1433 and 1385 cm^{-1} assignable to $\nu_5(NO_3)$ and

Table 2
Important IR spectral bands of H_2L and its metal complexes.

Compound	$\nu(NH)$	$\nu(C{=}O)$	$\nu(C{=}N)_{azo}$	$\nu(C{=}N)_{py}$	$\nu(C{=}N^*)$	$\nu(C{-}O)$	$\nu(N{-}N)$	$\nu(M{-}O)$	$\nu(M{-}N)$	$\nu(O{-}H)^*$
H_2L	3342	1693	1593	1575	–	–	1060	–	–	–
$[Cu(H_2L)(OAc)_2]\cdot H_2O$	–	1696	1598	1569	–	–	1061	568	456	3421
$[Cu_2(L)(OAc)_2(H_2O)_2]\cdot 3H_2O$	–	–	1603	1569	1630	1265	1097	564	457	3427
$[Co_2L(OAc)_2(H_2O)_2]\cdot H_2O$	–	–	1602	1563	1635	1259	1073	580	460	3411
$[Ni(HL)_2(H_2O)_2]\cdot H_2O$	2975	1700	1598	1565	1621	1321	1086	580	450	3420
$[Fe(H_2L)Cl_3]\cdot H_2O$	3296	1695	1622	1571	–	–	1065	550	465	3418
$[Cr(H_2L)Cl_3]\cdot 2H_2O$	3282	1691	1612	1563	–	–	1047	551	484	3438
$[Mn(H_2L)Cl_2(H_2O)]\cdot H_2O$	3282	1676	1614	1571	–	–	1068	555	460	3420
$[VO(H_2L)SO_4(H_2O)]\cdot 2H_2O$	3262	1691	1623	1593	–	–	1043	553	464	3420
$[Cd(HL)(AcO)EtOH]EtOH$	3399	1657	1569	1542	1617	1264	1057	591	464	–
$[Ag(H_2L)NO_3]\cdot H_2O$	3344	1705	1614	1580	–	–	1096	–	477	3434

$\nu(O{-}H)^*$ of H_2O.

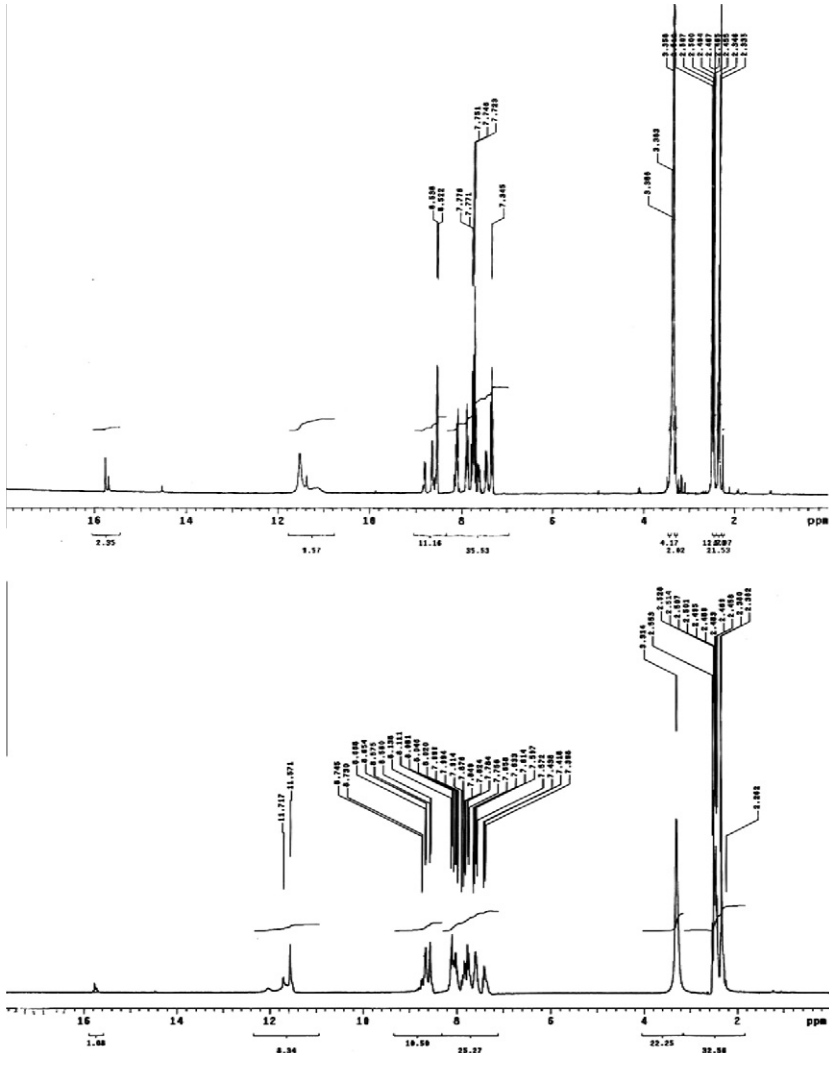

Fig. 1. ^{1}H NMR spectra of: (i) H_2L and (ii) $[Ag(H_2L)NO_3]·H_2O$.

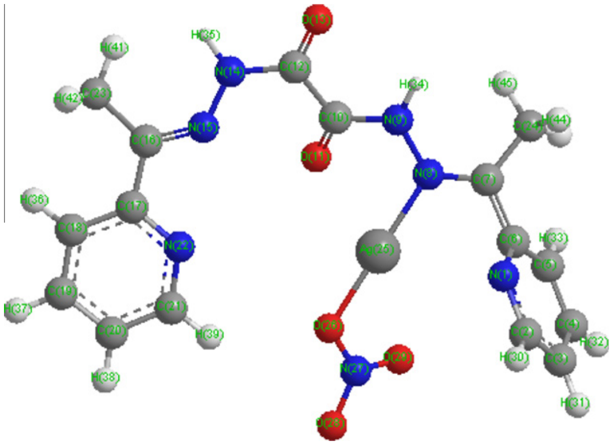

Structure 2. Molecular modeling of $[Ag(H_2L)(NO_3)]·H_2O$.

$\nu_1(NO_3)$ with difference ($\Delta\nu = 48\ cm^{-1}$) in agreement with the monodentate nature of NO_3 [29]. The neutral behavior of H_2L in $[Ag(H_2L)(NO_3)]·H_2O$ is supported by its ^{1}H NMR spectrum, in d_6-DMSO solution (Fig. 2) which shows the NH signals at 11.71 and 11.57 ppm.

In $[Fe(H_2L)(H_2O)Cl_3]·H_2O$, $[Cr(H_2L)Cl_3]·2H_2O$ and $[Mn(H_2L)Cl_2(H_2O)]·H_2O$ (Structures 3–5) H_2L behaves as a neutral NNO tridentate *via* $C{=}N_{azomethine}$, $C{=}N_{py}$ and C=O. This mode is revealed by the weakness of the $\nu(C{=}O)$ band suggesting that one C=O is involved in coordination. The shifts of $\nu(C{=}N)_{py}$ and $\nu(N{-}N)$ to higher wavenumbers and that of $\nu(C{=}N)_{azomethine}$ to lower wavenumber indicate the involvement of their nitrogens in bonding.

In $[Cu(H_2L)(OAc)_2]·H_2O$ and $[VO(H_2L)(SO_4)(H_2O)]·2H_2O$ (Structures 6 and 7), the ligand coordinates through $C{=}N_{azomethine}$ and one of the C=O groups. This mode is confirmed by the shifts of $\nu(C{=}N)_{azomethine}$ and $\nu(C{=}O)$ to higher and lower wavenumbers, respectively. The broad bands at 1542 and 1374 cm^{-1} assignable to $\nu_{as}(OCO)$ and $\nu_s(OCO)$ with difference ($\Delta\nu = 168\ cm^{-1}$) confirming the monodentate nature of the acetate group [30]. In $[VO(H_2L)SO_4(H_2O)]·2H_2O$, the bands at 1228, 1043, 989 and 464 cm^{-1} are due to ν_3, ν_1, ν_4 and ν_2 of sulfate suggesting its bidentate nature [31] while the band at 989 cm^{-1} is characteristic for $\nu(V{=}O)$ [32] which overlapped with ν_2 of sulfate.

The IR spectra of $[Cu_2(L)(OAc)_2(H_2O)_2]·3H_2O$ and $[Co_2L(OAc)_2(H_2O)_2]·H_2O$ (Structures 8 and 9) show that H_2L behaves as a dibasic NNONNO coordinating *via* the two $C{=}N_{azomethine}$, the two $C{=}N_{py}$ and the two enolized carbonyl groups. This behavior is supported by the disappearance of $\nu(C{=}O)$ with the appearance of $\nu(C{-}O)$ at 1259 cm^{-1} and the shifts of $C{=}N_{azomethine}$ to higher

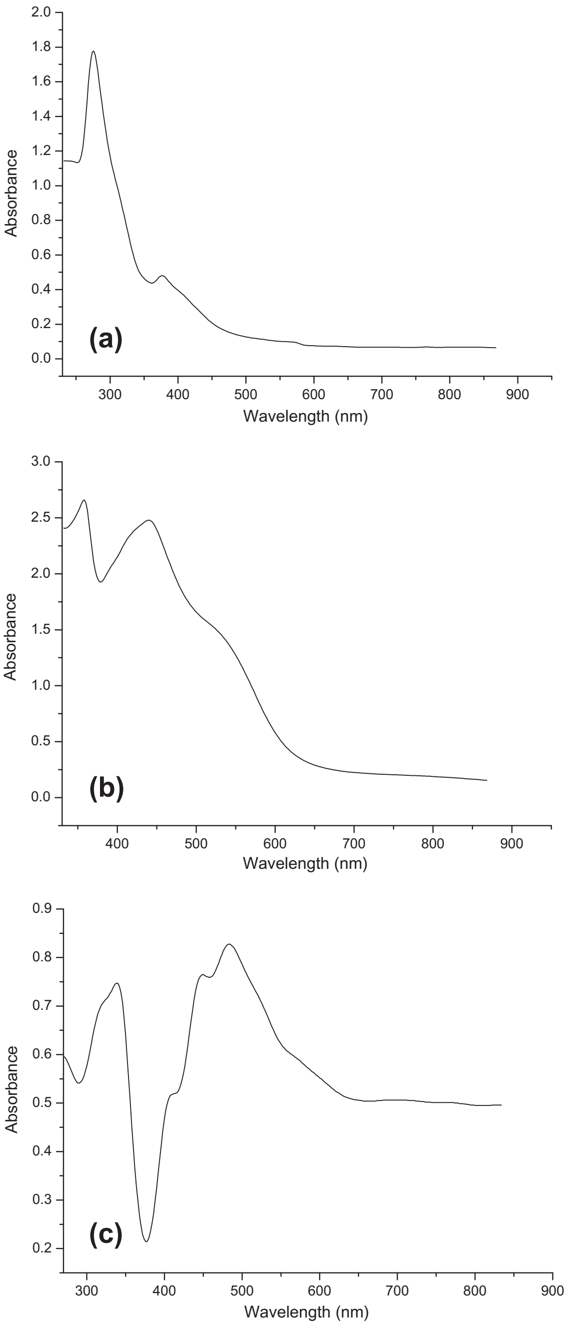

Fig. 2. Electronic spectra of: (a) $[Co_2(L)(OAc)_2(H_2O)_2]\cdot H_2O$, in DMF; (b) $[VO(H_2L)SO_4(H_2O)]\cdot 2H_2O$, in DMF and (c) $Mn(H_2L)Cl_2(H_2O)]\cdot H_2O$ in Nujol.

wavenumber and C=N$_{py}$ to lower wavenumber. Moreover, the new band at *ca.* 1630 cm^{-1} attributed to $\nu(N^{*}=C=C=N^{*})$ is an additional evidence for the enolization. The acetate group has bands at 1385 and 1265 cm^{-1} assignable to ν_{as}(OCO) and ν_s(OCO) with difference ($\Delta\nu$ = 120 cm^{-1}) [30] in a bidentate nature.

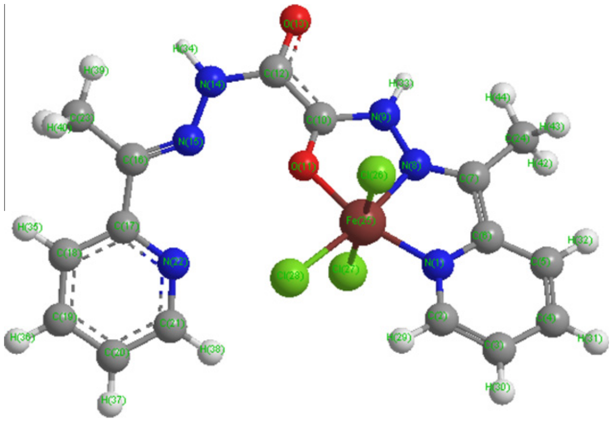

Structure 3. Molecular modeling of $[Fe(H_2L)(H_2O)Cl_3]\cdot H_2O$.

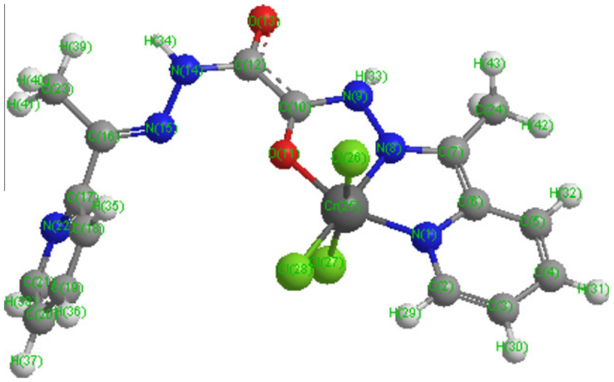

Structure 4. Molecular modeling of $[Cr(H_2L)Cl_3]\cdot 2H_2O$.

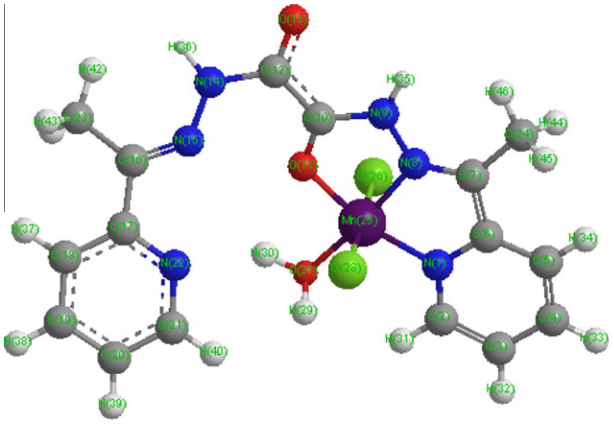

Structure 5. Molecular modeling of $[Mn(H_2L)Cl_2(H_2O)]\cdot H_2O$.

In $[Ni(HL)_2(H_2O)_2]\cdot H_2O$ (Structure 10), H_2L coordinates *via* =C—O— and NH groups acting as a monobasic bidentate supporting by the weakness and the shift of the bands due to ν(C=O) and ν(NH) to higher and lower wavenumbers, respectively. The IR spectrum of [Cd(HL)(OAc)(EtOH)]EtOH (Structure 11) indicates that H_2L coordinates in a mononegative bidentate through the two carbonyl groups (in keto and enol forms). This mode is supported by the shift of ν(C=O) (weak band) to lower wavenumber; the disappearance of ν(NH) and the appearance of new bands at 1617 and 1264 cm^{-1} due to $\nu(C=N^{*})$ and ν(C—O). The acetate group is bidentate by the appearance of 1542 and 1434 cm^{-1} bands with $\Delta\nu$ = 108 cm^{-1} [30]. New bands are observed in all complexes at 580–591 and 450–484 cm^{-1} assigned to ν(M—O) and ν(M—N) [33,34]. The broad bands at ≈3411–3438, 868–850, and ≈567 cm^{-1} in the IR spectra of complexes are referred to $\nu(H_2O)$, $\rho_r(H_2O)$ and ρ_w (H_2O) for the coordinated water while the broad band centered at ≈3500 cm^{-1} may be due to the hydrated water.

3.3. Electronic spectra and magnetic measurements

The electronic spectra of H_2L and its complexes were recorded in DMF and Nujol and the assignments of their bands, magnetic

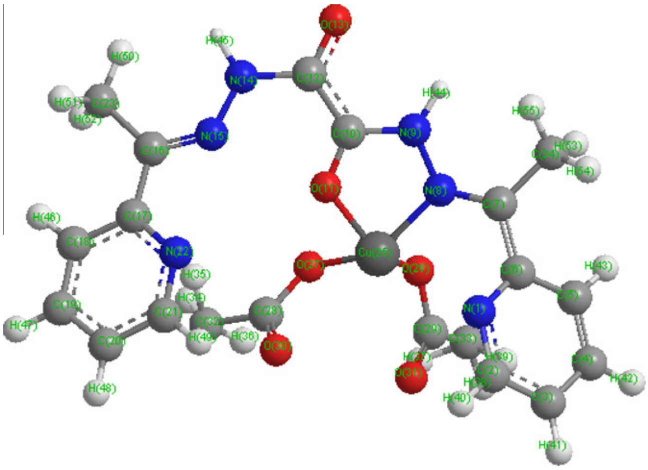

Structure 6. Molecular modeling of $[Cu(H_2L)(OAc)_2]{\cdot}H_2O$.

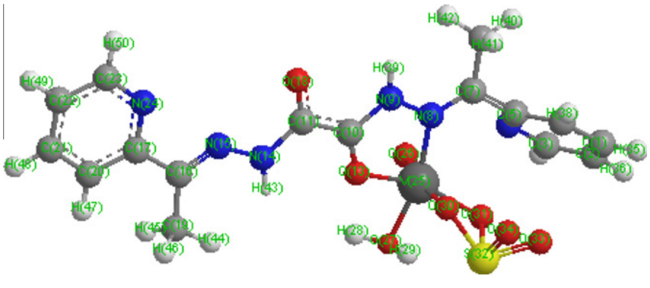

Structure 7. Molecular modeling of $[VO(H_2L)(SO_4)(H_2O)]{\cdot}2H_2O$.

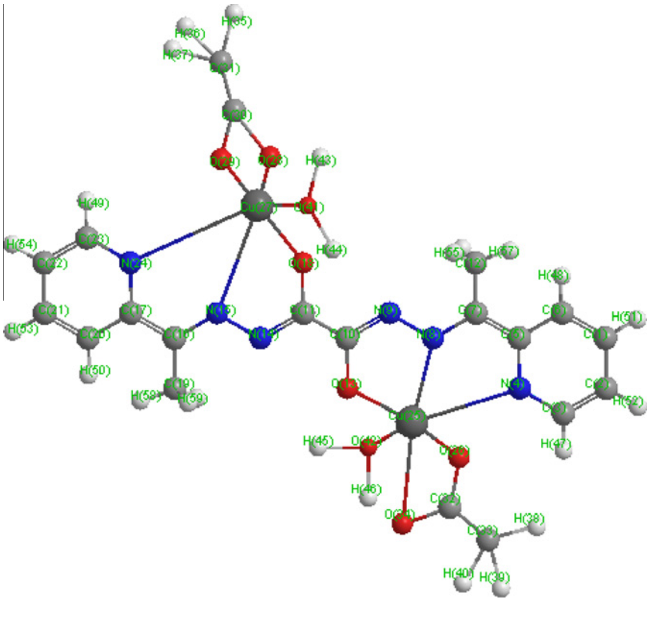

Structure 8. Molecular modeling of $[Cu_2L(OAc)_2(H_2O)_2]{\cdot}3H_2O$.

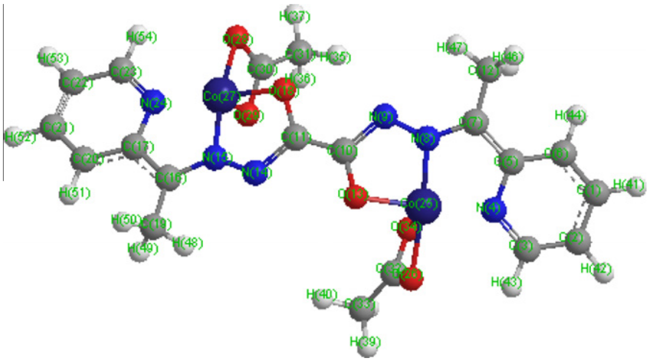

Structure 9. Molecular modeling of $[Co_2(L)(OAc)_2(H_2O)_2]{\cdot}H_2O$.

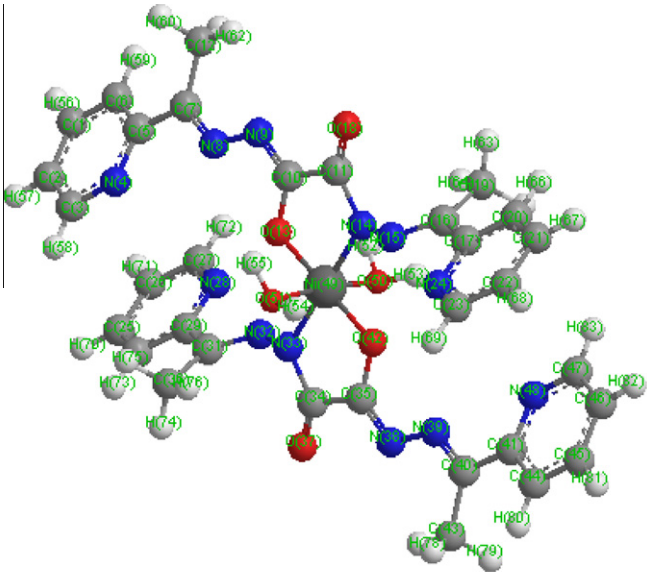

Structure 10. Molecular modeling of $[Ni(HL)_2(H_2O)_2]{\cdot}H_2O$.

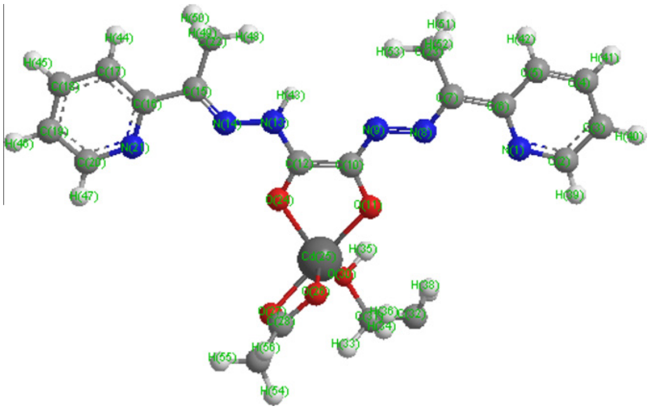

Structure 11. Molecular modeling of [Cd(HL)(OAc)(EtOH)]EtOH.

moments, molar absorptivity and the ligand field parameters are given in Table 3. The ligand spectrum showed a band at 40 323 cm^{-1} assigned to $\pi \rightarrow \pi^*$ and two strong bands at 34 722 and 26 596 cm^{-1} due to $n \rightarrow \pi^*$ of C=O and C=N. Large change is observed in the spectra of the complexes with a new $n \rightarrow \pi^*$ band at 36 496–33 557 cm^{-1} and $n \rightarrow \pi^*$ band at 26 316–27 933 cm^{-1}.

The electronic spectrum of $[Cu(H_2L)(OAc)_2]{\cdot}H_2O$ shows a broad band at 14 925 cm^{-1} due to $^2B_{1g} \rightarrow {}^2A_{1g}$ in a square–planar geometry [35–37]. The bands at 24 272 and 23 585 cm^{-1} may be due to LMCT [38]. The magnetic moment value (2.29 BM) is found higher

Table 3
Magnetic moments, electronic spectral bands, molar absorptivity and ligand field parameters of H_2L and its complexes.

Compound	μ_{eff} (B.M.)	Solvent	Intraligand and d–d transitions cm^{-1}	Molar absorptivity ($\varepsilon = L\ mol^{-1}\ cm^{-1}$)	Ligand field parameters		
					Dq (cm^{-1})	B (cm^{-1})	β
H_2L	–	DMF	40 323, 33 784, 34 722, 34 483, 26 596				
		Nujol	33 113, 22 831				
$[Cu(H_2L)(OAc)_2]\cdot H_2O$	2.29	DMF	33 560, 25 510, 23 585, 14 925	1057, 1105, 1375, 1084			
		Nujol	26 315, 25 000, 14 245				
$[Cu_2(L)(OAc)_2(H_2O)_2]\cdot 3H_2O$	3.20	DMF	36 495, 33 110, 26 315				
		Nujol	28 735, 24 390, 21 645, 19 230, 16 720, 14 045				
$[Co_2L(OAc)_2(H_2O)_2]\cdot H_2O$	2.57	DMF	36 495, 26 880, 13 475, 17 390				
		Nujol	37 035, 29 940, 25 640, 23 365, 18 550				
$[Ni(HL)_2(H_2O)_2]\cdot H_2O$	4.05	DMF	34 480, 27 625, 23 040, 17 540, 13 120		788.47	829.97	0.79
		Nujol	34 245, 31 055, 28 090, 25 770, 23 475				
$[Fe(H_2L)Cl_3]\cdot H_2O$	6.77	DMF	35 715, 32 260, 27 930, 24 630, 18 870, 15 245	2396, 2513, 2514, 2537, 1629, 162			
		Nujol	34 720, 28 090, 24 040, 21 010, 18 315				
$[Cr(H_2L)Cl_3]\cdot 2H_2O$	4.56	DMF	35 715, 32 465, 27 933, 24 155, 21 930, 17 545	2426, 2495, 2526, 2590, 1684, 1846,	1754.40	649.03	0.70
		Nujol	20 410, 16 290				
$[Mn(H_2L)Cl_2(H_2O)]\cdot H_2O$	7.12	DMF	27 930, 25 250, 24 390	2360, 2431, 2378			
		Nujol	310 055, 29 410, 24 270, 22 320, 20 830, 17 300				
$[VO(H_2L)SO_4(H_2O)]\cdot 2H_2O$	2.11	DMF	35 715, 32 895, 27 780, 22 830, 19 010	2347, 2519, 2358, 1825, 148			
		Nujol	33 785, 27 930, 22 625, 19 840, 17 605				
$[Cd(HL)(OAc)EtOH]EtOH$	–	DMF	33 330, 28 090	2310, 2485			
		Nujol	34 245, 29 070, 25 125, 21 835				
$[Ag(H_2L)NO_3]\cdot H_2O$	–	DMF	36 495, 33 555, 31 655, 29 410	2546, 2494, 2214, 124			
		Nujol	31 845, 28 735, 22 830				

The ε values are corresponding to the electronic transition bands.

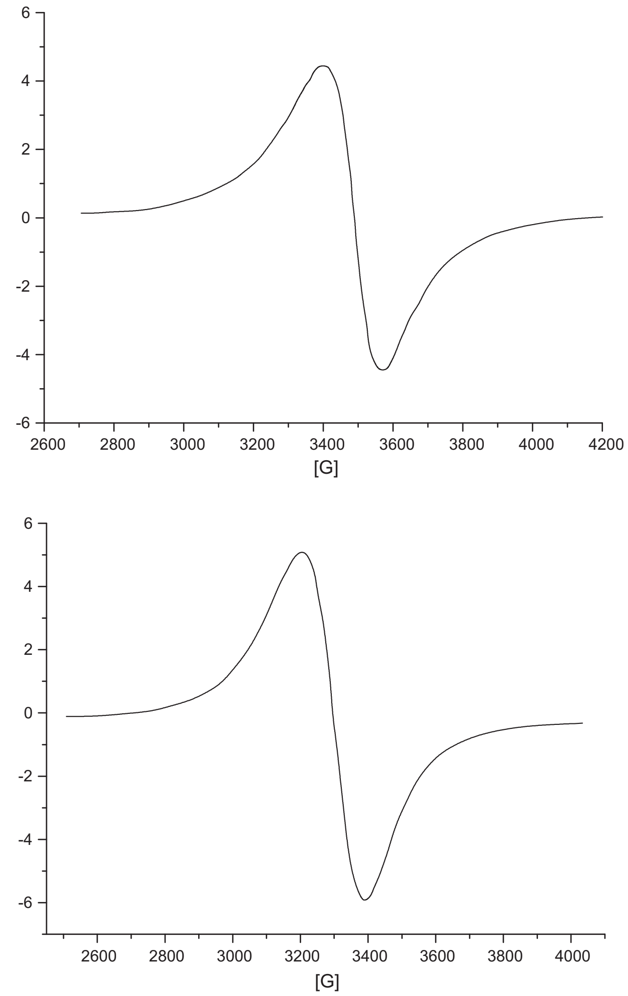

Fig. 3. ESR spectra of: (i) $[VO(H_2L)SO_4(H_2O)]\cdot 2H_2O$ and (ii) $[Cu(H_2L)(OAc)_2]\cdot H_2O$.

than the spin only value of the Cu(II) complexes referring to the spin–orbital coupling [39]. On the other hand, the electronic spectrum of $[Cu_2(L)(OAc)_2(H_2O)_2]\cdot 3H_2O$, in Nujol, shows bands at 16 722 and 14 044 cm^{-1} due to the d–d transition attributing to the six coordinate geometry [40].

The spectrum of $[Co_2(L)(OAc)_2(H_2O)_2]$. H_2O (Fig. 2a) shows a band at 17 391 cm^{-1} in DMF (18 549 cm^{-1} in Nujol) due to $^2B_{2g} \rightarrow {}^2A_{1g}$ and $^1A_{1g} \rightarrow {}^2A_{2g}$ in a square–planar Co(II) complex [41]. The magnetic moment value (2.57 BM) may suggest the existence of mixed stereochemistry confirming by two bands at 13 477 and 17 391 cm^{-1}. The second band is assigned to $^4A_2 \rightarrow {}^4T_1(F)$ (ν_3) in a tetrahedral geometry while the band at 23 364 cm^{-1} is due to a square–planar geometry [42].

The electronic spectrum of $[Ni(HL)_2(H_2O)_2]\cdot H_2O$ exhibits two bands at 17 544 and 23 041 cm^{-1} in DMF assignable to $^3A_{2g} \rightarrow {}^3T_{1g}$ (F) and $^3A_{2g} \rightarrow {}^3T_{1g}$ (P), respectively, in an octahedral structure [35,42]. The calculated values [Dq, B and β = 788.47 cm^{-1}, 829.97 cm^{-1} and 0.79] as well as the magnetic moment value are in accordance with the octahedral geometry.

The spectrum of the $[Fe(H_2L)(H_2O)Cl_3]\cdot H_2O$ exhibits bands at 15 244, 18 868 and 24 630 cm^{-1} attributed to $^6A_{1g} \rightarrow {}^4T_{1g}$(G), $^6A_{1g} \rightarrow {}^4T_{2g}$ (G) and $^6A_{1g} \rightarrow {}^4E_g$ (G), respectively, in an octahedral configuration [43]. The magnetic moment value (6.77 BM.) is a further support for the suggested geometry.

Table 4
Decomposition steps with the temperature range and weight loss for H_2L complexes.

Complex	Temp. range, °C	Removed species	Wt. loss	
			Found%	Calcd.%
$[Cu(H_2L)(OAc)_2]\cdot H_2O$	39–154	$-(H_2O)$	3.576	3.838
	208–339	$-(2OAC + C_5H_4N)$	37.410	37.439
	440–684	$-(C_5H_4N + CONH + CNH + 2CNCH_3)$	43.151	43.543
	685–800	(CuO) (residue)	15.863	15.180
$[Cu_2(L)(OAc)_2(H_2O)_2]\cdot 3H_2O$	41–121	$-2(H_2O)$	5.316	5.478
	122–177	$-(H_2O)$	2.745	2.739
	178–356	$-(2OAC + C_5H_4N + 2H_2O)$	35.756	35.312
	357–464	$-(C_5H_4N + 2CNCH_3 + 2CN)$	32.018	32.275
	464–800	2(CuO) (residue)	24.165	24.193
$[Co_2L(OAc)_2(H_2O)_2]\cdot H_2O$	38–130	$-(3H_2O)$	8.461	8.833
	315–496	$-(C_5H_4N + OAC + CNCH_3)$	29.055	29.102
	4967–616	$-(C_5H_4N + OAC + CNCH_3)$	29.055	29.102
	617–678	$-(2CN)$	8.471	8.490
	679–800	2CoO (residue)	24.463	24.473
$[Ni(HL)_2(H_2O)_2]\cdot H_2O$	25–76	$-(2H_2O)$	4.910	4.744
	77–230	$-(C_5H_4N + H_2O + CNCH_3)$	18.544	18.061
	231–400	$-(3C_5H_4N)$	29.991	30.851
	401–564	$(3CNCH_3 + 2CONH + CNO + CN)$	36.705	8.36.509
	565–800	NiO (residue)	9.850	9.835
$[Fe(H_2L)Cl_3]\cdot H_2O$	44–150	$-(H_2O)$	3.847	3.570
	151–301	$-(C_5H_4N + 2Cl)$	30.312	29.542
	302–477	$-(C_5H_4N + Cl + CNCH_3 + NH + 2CO)$	44.051	44.727
	478–590	$-(NH + CCH_3)$	8.471	8.335
	591–800	FeN (residue)	13.319	13.844
$[Cr(H_2L)Cl_3]\cdot 2H_2O$	43–136	$-(2H_2O)$	6.572	6.946
	251–385	$-(C_5H_4N + 3Cl)$	35.043	35.561
	386–500	$-C_5H_4N + CCH_3 + CNCH_3 + 2CONH)$	45.665	44.768
	501–800	CrN (residue)	12.720	12.724
$[Mn(H_2L)Cl_2(H_2O)]\cdot H_2O$	51–138	$-(H_2O)$	3.979	3.705
	139–280	$-(H_2O + Cl)$	9.872	10.996
	281–385	$-(C_5H_4N + Cl)$	23.286	23.352
	386–463	$-(CNCH_3 + CONH)$	17.665	17.291
	463–578	$-(C_5H_4N + CNCH_3 + CNH)$	30.588	30.062
	579–800	MnO (residue)	14.610	14.589
$[VO(H_2L)SO_4(H_2O)]\cdot 2H_2O$	74–122	$-2(H_2O)$	6.846	6.656
	237–482	$-(2C_5H_4N + CNCH_3 + CONH + 2H_20)$	48.035	47.709
	483–695	$-(CNCH_3 + CNH + SO_4)$	29.323	30.316
	696–800	VO_2 (residue)	15.796	15.319
Cd(HL)(OAc)EtOH]EtOH	40–143	−(EtOH)	7.187	7.849
	281–421	$-(EtOH + C_5H_4N + OAC)$	31.533	31.220
	646–791	$-(C_5H_4N + 2\ CNCH_3 + CONH + CN)$	39.608	39.053
	792–800	(CdO)(residue)	21.672	21.878
$[Ag(H_2L)NO_3]\cdot H_2O$	237–306	$-(2C_5H_4N + CNCH_3 + CONH + H_2O$	50.304	50.422
	557–696	$-(NO_3)$	12.156	12.104
	697–800	$(AgCNCH_3CONH)$(residue)	37.540	37.472

The electronic spectrum of $[Cr(H_2L)Cl_3]\cdot 2H_2O$ shows bands at 17 544 and 24 155 cm^{-1} assignable to $^4A_{2g} \rightarrow {}^4T_{2g}(F)$ (ν_1) and $^4A_{2g} \rightarrow {}^4T_{1g}(F)$ (ν_2), respectively in an octahedral geometry [44]. The $^4A_{2g} \rightarrow {}^4T_{1g}(P)$ (ν_3) band is expected to be at 32 470 cm^{-1}, generally overlapped with the charge transfer band. The B value is calculated by: $B = (2\nu_1^2 - 3\nu_1\,\nu_2 + \nu_2^2)/(15\nu_2 - 27\nu_1)$ [45] and the value β is computed as: $\beta = B/B^{\circ}$ ($B^{\circ} = 918\ cm^{-1}$). The calculated Dq, B, β and ν_2/ν_1 values as well as the magnetic moment (4.56 BM) confirm an octahedral environment.

The magnetic moment (2.11 B.M.) and the electronic spectrum of $[VO(H_2L)SO_4(H_2O)_2]–H_2O$ (Fig. 2b) is typical for octahedral VO^{2+} complexes as illustrated by the two bands at 22 831 and 19 011 cm^{-1} assignable to $^2B_2 \rightarrow {}^2E$ and $^2B_{2g} \rightarrow {}^2B_1$ [45,46].

The spectrum of $[Mn(H_2L)(H_2O)Cl_2]\cdot H_2O$ (Fig. 2c) exhibits bands at 17 300 and 20 830 cm^{-1} in Nujol due to $^6A_1g \rightarrow {}^4T_1g$ (G) and $^6A_1g \rightarrow {}^4T_2g$ (G), respectively in an octahedral geometry [47]. Also, the magnetic moment (7.12 BM) is consistent with that reported for a high spin d^5 system.

The spectrum of $[Ag(H_2L)NO_3]\cdot H_2O$ exhibits two bands at 36 496 and 31 654 cm^{-1} attributed to intraligand and charge transfer transitions. The shift of 26 596 cm^{-1} in the ligand spectrum to 29 411 cm^{-1} is an evidence for the participation of C═N in coordination [17].

3.4. Electron spin resonance

The solid state ESR spectra of $[Cu(H_2L)(OAc)_2]\cdot H_2O$ and $[VO(H_2L)SO_4(H_2O)_2]\cdot H_2O$ complexes (Fig. 3) showed only an intense and broad signal without hyperfine splitting with g_{iso} of 2.12 and 1.987, respectively. In case of Cu(II) complex, the shape of the spectrum is consistent with a square–planar environment and its higher g value comparing to that of the free electron ($g = 2.0023$) revealing an appreciable covalency of the metal ligand bonding with $dx^2 - y^2$ as the ground-state [48] characteristic of square planar or square pyramidal or octahedral stereochemistry [49]. From structurally copper complexes of thiosemicarbazides

Table 5
Effect of water and some organic solvents on the ligand.

Solvent	Bands (nm)	Concentration, M	Molar absorpitivity (ε) $mol^{-1}\ L \times 10^4$
Water	222, 240, 292, 300, (318)	–	–
Methanol	218, 280, 314, (330)	3×10^{-4}	0.80, 0.90, 0.82, 0.63
Ethanol	224, 296, 318, (332)	–	–
Benzene	288, 302, 318, (342)	–	–
DMF	276, 286, 318, 340, (350)	–	–
DMSO	240, 298, 318, (344)	1.5×10^{-4}	0.73, 0.12, 0.15, 0.14

ε Value is calculated for the band between brackets.

Table 6
Antibacterial activities in terms of inhibition zone diameter (mm) of H_2L and its metal complexes.

Compound	Zone of inhibition of bacterial growth (mm)	
	Bt (Gram-positive)	*Pseudomonas* (Gram-negative)
H_2L	0	0
$[Ag(H_2L)NO_3]\cdot H_2O$	12	18
$[Cr(H_2L)Cl_3]\cdot 2H_2O$	0	0
$[Cu\ (H_2L)(OAc)_2]\cdot H_2O$	20	0
$[VO(H_2L)SO_4\cdot H_2O]\cdot 2H_2O$	7	0

[50], it has been observed that the increase in $g_{||}$ value with concomitant decrease in ${}^{Cu}A_{||}$ component leads to an increase in the tetrahedral distortion. The degree of distortion, $f(\alpha) = g_{||}/A_{||}$ for the complex (119 cm^{-1}) lies within the range expected for a square planar geometry [51]. The ESR spectrum of the VO^{2+} complex is isotropic with g_{iso} lower than the free-electron value (2.0023) as expected for the d^1-system with an octahedral arrangement related to the spin–orbit interaction of the ground state with a low-lying excited state. This decrease in the free-electron value reveals a strong ligand field strength [52].

3.5. Mass spectra

The successive fragmentation of H_2L is illustrated in Scheme 1. The molecular ion peak (3 2 4) is typical with the calculated molecular weight (324.337). The end fragment (5 4 0) may be corresponding to C_4H_6.

3.6. Thermogravimetric studies

The stages of decomposition, temperature range, decomposition product as well as the weight loss percentages of some complexes are given in Table 5. Fig. 3 shows the TGA curve of $[Cu(H_2L)(OAc)_2]\cdot H_2O$ as a representative example. The thermogram displays three degradation steps at 39–154, 208–339 and 440–684 °C with weight losses of 3.57 (Calcd. 3.84%), 37.41 (Calcd. 37.41%) and 43.1 (Calcd. 43.5%) corresponding to the loss of H_2O, 2OAC + C_5H_4N and C_5H_4N + CONH + CNH + $2CNCH_3$ species. The residual part is CuO (Found 15.9; Calcd. 15.2%).

An inspection of the data represented in Table 4 indicates that the TG thermogram displayed a high residual part for the studied complexes revealing high stability of the formed chelates.

3.7. Effect of pH on the ligand

The effect of pH on H_2L was investigated at pH 2–12 by recording the spectra of 3.9×10^{-4} mol L^{-1} in universal buffer solutions; at 300 and 322 nm. The pK's of the ligand were calculated by the half-height method (absorbance–pH curves) giving different pK values. In DMSO, the pK's obtained were 4.16, 7.00, 9.03 and 5.7, 9.6 at 300 and 322 nm, respectively due to the two amide protons. In MeOH, the values are 7.16 and (4.60, 9.00) at 3 0 0 and (3 2 2) nm while in H_2O; one value (7.16) is obtained at the chosen wavelengths. The data are consistent with those obtained previously [16]. One can observe that in different solvents a different number of pK's are determined and the value at *Ca.* 7.00 is commonly calculated in the different solvents.

3.8. Effect of solvents on the ligand

The effect of H_2O, EtOH, MeOH, benzene, DMF and DMSO on the spectrum of H_2L is illustrated in Table 3. In H_2O, five bands are observed at 222, 240, 292, 300 and 318 nm. The spectrum in benzene shows bands at 288, 302, 318 and 342 nm. The change of the spectrum from H_2O to benzene may be attributed to the formation of hydrogen bonding with H_2O or solvent polarity effect. The hydrogen bond strength is calculated from the difference between 318 and 342 nm (24 nm = 41 666 cm^{-1}) [17]. The molar absorptivity in MeOH and DMSO are shown in Table 5. The last band may arrange the solvents as: $H_2O < CH_3OH < C_2H_5OH < C_6H_6 <$ DMSO < DMF according to the polarity of the solvents.

3.9. Antimicrobial activity

The biological activity of H_2L and its Cu^{2+}, Cr^{3+}, VO^{2+}, Ag^+ complexes against *B. thuringiensis* (*Bt*) and *P. aeuroginosa* (*Pa*) is summarized in Table. Examining the values for Gram's positive bacteria in Table 6, one can arrange the compounds as: $[Cu(H_2L)(OAc)_2]\cdot H_2O > [Ag(H_2L)NO_3]\cdot H_2O > [VO(H_2L)SO_4(H_2O)]\cdot 2H_2O$ and only $[Ag(H_2L)NO_3]\cdot H_2O$ complex exhibited an inhibition effect against *Pa* organism. It is known that, the coordination number, solubility and the hydrophobicity of the complex governs the antimicrobial activity. In the present case, the activity is strongly denendent on the central metal ion and its ability to diffuse into the cell membrane of the organism.

4. Conclusion

$N^{1'},N^{2'}$-bis[1-(pyridin-2-yl)ethylidene]oxalo hydrazide (H_2L) and its complexes with Cr^{3+}, Mn^{2+}, Fe^{3+}, Co^{2+}, Ni^{2+}, Cu^{2+}, Cd^{2+}, VO^{2+} and Ag^+ have been characterized. The ligand pK's are 4.62, 7.78 and 9.45. The ligand behaves as neutral (mono- or dibasic) bidentate, tridentate or tetradentate. Cr^{3+}, Mn^{2+}, Fe^{3+}, Ni^{2+} and VO^{2+} form octahedral complexes while Co^{2+} and Cu^{2+} form square–planar. $[VO(H_2L)SO_{4\_}(H_2O)_2]\cdot H_2O$ and $[Cu(H_2L)(OAc)_2]\cdot H_2O$ are mononuclear species. No effect was observed for the complexes on Pa bacteria growth except for $[Ag(H_2L)(NO_3)]H_2O$ which had a high activity; Cu^{2+} exhibits a high activity against BT.

Appendix A. Supplementary material

Supplementary data associated with this article can be found, in the online version, at doi:10.1016/j.molstruc.2011.04.043.

References

[1] A.A. Abou-Hussen, I.M. Saad, A.A. El-Asmy, J. Coord. Chem. 58 (2005) 1735.
[2] J.S. Casas, M.S. Garcia-Tasende, J. Sordo, Coord. Chem. Rev. 209 (2000) 197.
[3] N.M. El-Metwally, G.A. Al-Hazmi, A.A. El-Asmy, Transition Met. Chem. 31 (2006) 673.
[4] T.S. Lobana, R. Sharma, G. Bawa, S. Khanna, Coord. Chem. Rev. 253 (2009) 977.
[5] H. Beraldo, D. Gambino, Mini-Rev. Med. Chem. 4 (2004) 31.
[6] M.B. Ferrari, F. Bisceglie, G.G. Fava, G. Pelosi, P. Tarasconi, R. Albertini, S. Pinelli, J. Inorg. Biochem. 89 (2002) 36.

[7] H.S. Seleem, B.A. El-Shetary, S.M.E. Khalil, M. Mostafa, M. Shebl, J. Coord. Chem. 58 (2005) 479.
[8] M.A. Akl, D.S. Ismael, A.A. El-Asmy, Microchem. J. 83 (2006) 61.
[9] E.M. Saad, M.S. El-Shahwai, H. Saleh, A.A. El-Asmy, Transition Met. Chem. 32 (2007) 155.
[10] H.G. Petering, H.H. Burskirk, J.A. Crim, Cancer Res. 27 (1967) 1115.
[11] D.R. McMillian, H.R. Engeseth, K.D. Karlin, J. Zubicta (Eds.), Biological and Inorganic Copper Chemistry, Adenine Press, Guilderland, NY, 1986.
[12] E. Bouwman, W.L. Driessen, J. Reedjik, Coord. Chem. Rev. 104 (1990) 143.
[13] D.X. West, A.B. Liberta, S.B. Padhye, R.C. Chikate, P.B. Sonawane, A.S. Kumbhar, R.G. Yerande, Coord. Chem. Rev. 123 (1993) 49.
[14] K. Wada, Y. Fujibayahsia, A. Yokoyama, Arch. Biochem. Biophys. 310 (1944) 1.
[15] L. Alsop, A.R. Cowly, J.R. Dilworth, P.S. Donnely, J.M. Peach, J.T. Rider, Inorgan. Chim. Acta 358 (2005) 2770.
[16] A.A. El-Asmy, A.Z. Al-Abdeen, W.M. Abo El-Maaty, M.M. Mostafa, Spectrochim. Acta 75 (A) (2010) 1516.
[17] A.A. El-Asmy, M.A. Abdallah, Sh.A. Mandour, K.M. Ibrahim, Inorg. Met. Org. Nano-Met. Chem. 40 (2010) 675.
[18] W.J. Geary, Coord. Chem. Rev. 7 (1971) 81.
[19] C.H. Collins, P.M. Lyne, R.D. Gillard, J.A. McCleverty (Eds.), Microbiological Methods, University Park Press, Baltimore, MD, 1970.
[20] HyperChem Version 8.0 Hypercube, Inc.
[21] O.A. El-Gammal, Spectrochim. Acta 75 (A) (2010) 533.
[22] A.A.R. Despaigne, J.G.D. Silva, A.C.M.D. Carmo, O.E. Piro, E.E. Castellano, H. Beraldo, J. Mol. Struct. 920 (2009) 97.
[23] S. Sagdinc, B. Koksoy, F. Kandemirli, S.H. Bayari, J. Mol. Struct. 917 (2009) 63.
[24] A.A. R Despaigne, J.G.D. Silva, A.C.M.D. Carmo, F. Sives, O.E. Piro, E.E. Castellano, H. Beraldo, Polyhedron 28 (2009) 3797.
[25] N.L. Alpert, W.E. Keiser, H. Szmanski, A Theory and Practice of Infrared Spectroscopy, Plenum Press, New York, 1970.
[26] P.B. Sreeja, M.R.P. Kurup, A. Kishore, C. Jasmin, Polyhedron 23 (2004) 575.
[27] U. El-Ayaan, G.A. EL-Reash, I.M. Kenawy, Synth. React. Inorg. Met. Org. Chem. 33 (2003) 329.
[28] T.R. Todorovic, U. Rychlewska, B. Warzajtis, D.D. Radanovic, N.R. Filipovic, I.A. Pajic, D.M. Sladic, K.K. Andelkovic, Polyhedron 28 (2009) 2397.
[29] L.J. Bellamy, The Infrared Spectra of Complex Molecule, Methuen, London, 1985.
[30] K. Nakamoto, Infrared Spectra of Inorganic and Coordination compounds, Third ed., Wiley, New York, 1970.
[31] H.M. E1-Shaaer, P. Foltinova, M. Lacova, J. Chovancova, H. Stankovicova, Il. Farmaco. 53 (1998) 224.
[32] M.H. Hamada, O. El-Shafai, A.A. El-Asmy, Transition Met. Chem. 31 (2006) 714.
[33] J.R. Ferraro, Low Frequency Vibrations of Inorganic and Coordination Compounds, Plenum Press, New York, 1971.
[34] J.R. Ferraro, W.R. Walkers, Inorg. Chem. 4 (1965) 1382.
[35] A.B.P. Lever, Inorganic Electronic Spectroscopy, Elsevier, Amsterdam, 1984.
[36] A.A. El-Asmy, G.A. Al-Hazmi, Spectrochim. Acta 71A (2009) 1885.
[37] M. Pulaunianiandarvr, C. Natarajan, Aust. J. Chem. 33 (1985) 373.
[38] R.B. Wilson, J.R. Wasson, W.E. Hatfield, D.J. Hodgson, Inorg. Chem. 17 (1978) 641.
[39] J.C. Bailar, H.J. Emeleus, R. Nyholm, A.F. Trotman-Dickenson, Comprehensive Inorganic Chemistry, third ed., Pergamon Press, New York, 1975.
[40] S. Sharma, F. Athar, M.R. Maurya, F. Naqvi, A. Azam, Eur. J. Med. Chem. 40 (2005) 557.
[41] M.T.H. Tarafder, K. Chew, K.A. Crouse, A.M. Ali, B.M. Yamin, H.K. Fun, Polyhedron 21 (2002) 2683.
[42] A.A. El-Asmy, K.M. Ibrahim, M.M. Bekheit, M.M. Mostafa, Synth. React. Inorg. Met. -Org. Chem. 15 (1985) 287.
[43] S. Anuradha, S. Pramila, Indian J. Chem. 39A (2000) 874.
[44] P.G. Centre, T.G. Narenda, B.N. Murthy, Indian J. Chem. 28A (1989) 689.
[45] E.R. Price, J.R. Wasson, J. Inorg. Nucl. Chem. 36 (1974) 67.
[46] P. Manikandan, R. Muthukumaran, K.R.J. Thomas, B. Varghes, G.V.R. Chandramouli, P.T. Manoharan, Inorg. Chem. 40 (2001) 2378.
[47] M. Mohan, M. Kumar, Transition Met. Chem. 10 (1985) 255.
[48] M.V. Angleusiu, S.F. Barbuceanu, C. Draghici, G.L. Almajan, Eur. J. Med. Chem. 45 (2010) 2055.
[49] F.A. Cotton, G. Wilkinson, Advanced Inorganic Chemistry, fourth ed., John Wiley and Sons, New York, 1986.
[50] R.C. Chikate, A.R. Belapure, S.B. Padhye, D.X. West, Polyhedron 24 (2005) 889.
[51] S. Chandra, L.K. Gupta, Spectrochim. Acta A 62 (2005) 1102.
[52] O.P. Pandy, Polyhedron 5 (1986) 1587.